

Exploring Source and Detector Non-Standard Neutrino Interactions at ESS ν SB

Mattias Blennow,^{1,*} Sandhya Choubey,^{1,2,†} Tommy Ohlsson,^{1,‡} and Sushant K. Raut^{1,§}

¹*Department of Theoretical Physics,
School of Engineering Sciences, KTH Royal Institute of Technology,
AlbaNova University Center, 106 91 Stockholm, Sweden*

²*Harish-Chandra Research Institute,
Chhatnag Road, Jhansi, Allahabad 211 019, India*

Abstract

We investigate source and detector non-standard neutrino interactions at the proposed ESS ν SB experiment. We analyze the effect of non-standard physics at the probability level, the event-rate level and by a full computation of the ESS ν SB setup. We find that the precision measurement of the leptonic mixing angle θ_{23} at ESS ν SB is robust in the presence of non-standard interactions, whereas that of the leptonic CP-violating phase δ is worsened at most by a factor of two. We compute sensitivities to all the relevant source and detector non-standard interaction parameters and find that the sensitivities to the parameters $\varepsilon_{\mu e}^s$ and $\varepsilon_{\mu e}^d$ are comparable to the existing limits in a realistic scenario, while they improve by a factor of two in an optimistic scenario. Finally, we show that the absence of a near detector compromises the sensitivity of ESS ν SB to non-standard interactions.

* Email Address: emb@kth.se

† Email Address: sandhya@hri.res.in

‡ Email Address: tohlsson@kth.se

§ Email Address: raut@kth.se

I. INTRODUCTION

Without comparison, the Standard Model of particle physics (SM) is the most successful physics model to date, accurately predicting an enormous number of observables with high precision from only a handful of fitted parameters. The success of the SM may have culminated in 2012 when the ATLAS and CMS experiments announced the discovery of the Higgs boson [1, 2], predicted by the SM as a direct result of the electroweak symmetry breaking which was introduced to provide masses into the theory. Still, there are a number of observations which may not be explained within the SM itself. Most notable among these are the existence of dark matter, the exclusion of gravity and the observation of neutrino oscillations. In addition, there are conceptual theoretical problems with the SM, such as the hierarchy problem, indicating that the SM may only be a low-energy approximation of a more general theory. As such, the SM should be viewed as an effective theory and a priori higher-dimensional operators, suppressed by powers of a new mass scale Λ should be added to the SM Lagrangian. At lower energies, the additional effective operators will generally produce very small corrections due to this suppression. This concept is further supported by the fact that the only gauge invariant operator allowed at dimension five, and therefore suppressed only by one power of Λ , is the so-called Weinberg operator [3], which results in a Majorana mass term for the left-handed neutrinos of the SM. It is therefore not unreasonable to imagine that the effect of neutrino masses would be among the first observations of physics beyond the SM, which indeed is the case due to neutrino oscillations requiring neutrino mass-squared differences to be non-zero.

Neutrino flavour conversion, although at that time not confirmed as such, was first observed in solar neutrino experiments where a discrepancy between the observed flux and the flux predicted by solar models was found [4]. Since the first robust evidence of neutrino oscillations by the Super-Kamiokande experiment's observation of atmospheric neutrinos in 1998 [5], they have been extensively studied experimentally in a variety of atmospheric, solar, reactor, and accelerator experiments, which have helped to constrain the neutrino mass and mixing parameters to very high precision (see Refs. [6–8] for recent global fits). The remaining questions in neutrino oscillation physics today are the neutrino mass ordering, the existence or non-existence of CP violation in the lepton sector and the octant of the leptonic mixing angle θ_{23} . Answering these three questions is the main aim of the next gen-

eration of neutrino oscillation experiments, such as the European Spallation Source Neutrino Super-Beam (ESS ν SB) experiment [9], which is a proposed accelerator neutrino experiment based on the European Spallation Source (ESS) currently under construction in Lund, Sweden. The sensitivity of ESS ν SB to the CP-violating phase δ was studied in Ref. [9], while the sensitivity to other standard oscillation parameters was discussed in Ref. [10] and the sensitivity to light sterile neutrinos in Ref. [11].

While the Weinberg operator provides the neutrino masses necessary for neutrino oscillations to occur and neutrino oscillations have been firmly established as the leading mechanism behind neutrino flavour conversion, higher-order operators may give rise to sub-leading contributions to the neutrino conversion probabilities and their observation would allow us to gain additional insight into the high-energy completion of the SM and the generation of neutrino masses. In addition, it may be necessary to consider the robustness of the usual neutrino oscillation parameters when higher-order operators are also considered. One of the more common types of operators to be investigated in this respect is non-standard neutrino interactions (NSIs), which are effective four-fermion operators involving at least one neutrino field. For recent reviews on NSIs, see Refs. [12, 13].

In this work, we will consider the possible impact of NSIs at the ESS ν SB experiment. We will study both the influence of NSIs on the determination of the standard neutrino oscillation parameters and the bounds which ESS ν SB could place on the NSI parameters. In particular, we will focus on correlations in the determination of the leptonic CP violation and the NSI parameters, which is of large importance for ESS ν SB as the discovery of leptonic CP violation is the major scientific target of this experiment.

The rest of this work is organized as follows. In Sec. II, we will briefly review non-standard neutrino interactions and present the current upper bounds on the source and detector NSI parameters. Next, in Sec. III, the setup of the proposed ESS ν SB experiment will be discussed. Then, in Sec. IV, we will investigate the phenomenology of source and detector NSIs at probability and event-rate levels. In Sec. V, the main results of our full computation on source and detector NSIs at ESS ν SB will be presented. Finally, in Sec. VI, we will summarize and draw our conclusions.

II. NON-STANDARD NEUTRINO INTERACTIONS

When considering NSIs, we will be confronted with effective four-fermion operators of the type

$$\mathcal{O} = (\bar{f}_1 \gamma^\mu P_{L,R} f_2)(\bar{f}_3 \gamma_\mu P_{L,R} f_4) + h.c. , \quad (1)$$

where f_i ($i = 1, 2, 3, 4$) are SM fermion fields and $P_{L,R}$ are left- and right-handed projections. These operators are of dimension six and they will therefore appear together with an effective coupling constant of dimension minus two in the effective Lagrangian. Since we are interested in the NSIs of neutrinos, we require that at least one of the fermion fields in the operators is a neutrino field, which implies that the corresponding projection operator must be P_L . Furthermore, in order to keep the electromagnetic and strong interactions unbroken, we require that all operators are scalars under transformations of the corresponding gauge groups. Due to the weak interaction being broken, we do not impose any constraints on the transformation of the operators under $SU(2)_L$. It should be mentioned that imposing $SU(2)_L$ gauge symmetry on the dimension-six operators would lead to flavour constraints on these operators [14, 15], leaving only a few possible operators without significant constraints due to the non-observation of effective four-charged-fermion processes such as $\mu \rightarrow 3e$. The dimension-six operators which break $SU(2)_L$ may generally be induced from higher-dimensional operators such as $(\phi\phi^\dagger)\mathcal{O}$, where ϕ is the Higgs field, which are invariant under $SU(2)_L$, but generate $SU(2)_L$ -breaking terms once the Higgs field takes on a vacuum expectation value v . Depending on the dimension at which the NSIs are generated above the electroweak scale, we may expect the NSI coefficients to scale as v^{n-6}/Λ^{n-4} , where n is the dimension and Λ is the energy scale at which the NSIs are generated.

The different possible neutrino NSIs are generally divided into two categories of effective four-fermion operators. The neutral-current NSIs [16, 17]

$$\mathcal{O}_{\alpha\beta}^{f(L,R)} = (\bar{\nu}_\alpha \gamma^\mu P_L \nu_\beta)(\bar{f} \gamma_\mu P_{L,R} f) + h.c. , \quad (2)$$

where f is a charged fermion field, affects the neutrino flavour propagation in matter for $f = u, d, e$ by providing an effective potential analogous to the Mikheyev–Smirnov–Wolfenstein (MSW) potential [16, 18, 19]. For the neutral-current NSIs to be of importance, relatively large matter potentials and/or high neutrino energies are required. As this is not the case for the ESS ν SB experiment, we will not focus on such NSIs in this work. On the other hand,

the charged-current NSIs [20]

$$\mathcal{O}_{\alpha\beta}^{ff'(L,R)} = (\bar{\ell}_\alpha \gamma^\mu P_L \nu_\beta) (\bar{f} \gamma_\mu P_{L,R} f') , \quad (3)$$

where f and f' are different fermion fields such that the operator is invariant under $U(1)_{\text{EM}}$ and $SU(3)_c$, will instead affect the production and detection processes of neutrinos and this effect will not depend on the neutrino energy or the presence of matter along the neutrino propagation.

In the remainder of this work, we will focus on the charged-current NSI Lagrangian

$$\mathcal{L}_{\text{NSI}} = -2\sqrt{2}G_F \sum_{X \in \{L,R\}} \sum_{\alpha,\beta} \varepsilon_{\alpha\beta}^A (\bar{\nu}_\beta \gamma^\mu P_L \ell_\alpha) (\bar{d} \gamma_\mu P_X u) + h.c. , \quad (4)$$

which includes the operators that will appear in neutrino production by pion decays $\pi \rightarrow \ell_\alpha \nu$ and charged-current neutrino detection processes. Here, we have normalised the strength of the NSIs to that of the weak interaction by the introduction of the Fermi coupling constant G_F . The NSI parameters $\varepsilon_{\alpha\beta}$ are therefore dimensionless numbers expected to be of the order $(v/\Lambda)^{n-4}$. With the introduction of charged-current NSIs, the production amplitude of the neutrino mass eigenstate $|\nu_i\rangle$ in the π^+ , which in the SM is proportional to $U_{\mu i}^*$, where U is the leptonic mixing matrix, is now instead proportional to $\sum_\alpha (\delta_{\mu\alpha} + \varepsilon_{\mu\alpha}^s) U_{\alpha i}^*$, where the NSI parameters relevant for the source process are

$$\varepsilon_{\alpha\beta}^s = \varepsilon_{\alpha\beta}^R - \varepsilon_{\alpha\beta}^L . \quad (5)$$

Unlike the source process, the detection process does not necessarily involve a pseudoscalar current in the quark sector. We instead define the NSI parameters relevant for the detection process as

$$\varepsilon_{\alpha\beta}^d = (\varepsilon_{\beta\alpha}^P)^* , \quad (6)$$

where P represents the quark current in the detection process. Due to the nature of the inverse beta decay involved in the detection process, this definition oversimplifies the neutrino oscillation probabilities that we will discuss in Sec. IV.¹ However, we will use this as

¹ In fact, the neutrino oscillation probabilities should be computed along the lines

$$P_{\alpha\beta} \simeq \frac{1}{5.5} [P_{\alpha\beta}(\varepsilon^A, \varepsilon^V) + 4.5 P_{\alpha\beta}(\varepsilon^A, \varepsilon^A)] ,$$

where $P_{\alpha\beta}(\varepsilon^s, \varepsilon^d)$ is the probability for a given source/detector NSI. Note that the largest prefactor comes from the contribution with the source and detector effects both dependent on the axial quark current. This would therefore indicate a relation between the source and detector NSIs.

a simplified model for how NSIs may affect ESS ν SB. The complex conjugate and change of indices has been introduced to adhere to the usual convention in the field when considering detector NSI effects. The production rates of charged leptons at the detector in any neutrino oscillation experiment will be affected by this change in the production and detection amplitudes and we may ask the question whether or not the presence of such NSIs could be measured or have a negative impact on the experimental precision to the standard oscillation parameters. The experimental bounds (at the 90% C.L.) on the NSI parameters relevant for the ESS ν SB experiment from non-oscillation experiments are given by [21]

$$\begin{aligned}
|\varepsilon_{\mu e}^s| &< 0.026, & |\varepsilon_{\mu\mu}^s| &< 0.078, & |\varepsilon_{\mu\tau}^s| &< 0.013, \\
|\varepsilon_{ee}^d| &< 0.041, & |\varepsilon_{\mu e}^d| &< 0.025, & |\varepsilon_{\tau e}^d| &< 0.041, \\
|\varepsilon_{e\mu}^d| &< 0.026, & |\varepsilon_{\mu\mu}^d| &< 0.078, & |\varepsilon_{\tau\mu}^d| &< 0.013.
\end{aligned} \tag{7}$$

Although these bounds are quite stringent, it should be kept in mind that the next generation of neutrino experiments is aiming for highly sensitive measurements of the neutrino oscillation parameters. As such, even sub-leading effects may be of interest and it is worth the effort to examine the possible impact of these effects. It is also worth noting that new oscillation experiments, such as those performed with nuclear reactors, may be sensitive to some of these NSI parameters as well [22]. However, the current bounds from these experiments are somewhat weaker than the bounds quoted above [23].

III. THE ESS ν SB EXPERIMENTAL SETUP

In this section, we describe the experimental setup for the proposed ESS ν SB experiment. We have used the standard flux (with 2 GeV protons) and cross-sections from the ESS ν SB collaboration [9]. The source provides a neutrino beam for two years and an antineutrino beam for eight years. We have assumed that a 500 kiloton water Cherenkov detector is placed at a distance of 540 km from the source, which corresponds to the location of the mine in Garpenberg, Sweden. The detector specifications have been taken from the performance study of the MEMPHYS detector [24]. The energy range of interest is up to 2 GeV, which is divided into 20 energy bins. We have used 9% (18%) systematic errors on the signal (background) events. Unless specified otherwise, we have also assumed the existence of a near detector with mass 1 kiloton, 1 km from the source and the same flux as at the detector

at 540 km scaled by the distance-squared. As a crude approximation, we assume the same characteristics for both these detectors.

To this end, we have written our own probability engine to calculate the neutrino oscillation probability in the presence of source and detector NSIs. This probability engine interfaces with GLoBES [25, 26] for calculating the neutrino event rates at ESS ν SB. The large parameter space is handled with the help of the GLoBES plugin MonteCUBES [27].

IV. NEUTRINO OSCILLATIONS WITH NSIS

Standard three-flavour neutrino oscillations depend on six fundamental parameters – two mass-squared differences, Δm_{21}^2 and Δm_{31}^2 , three mixing angles, θ_{12} , θ_{13} and θ_{23} and one CP-violating phase δ . In addition, if the neutrinos are propagating through matter, the charged-current interactions of the neutrinos with electrons modify the oscillations. This effect can be incorporated into the probability formalism by using the MSW potential term $A = 2\sqrt{2}G_F n_e E$ [16, 18, 19], where n_e is the number density of electrons in the matter and E is the neutrino energy. For an experiment like ESS ν SB with a short baseline length as well as low neutrino energy, we can ignore the matter effects for the sake of this discussion. (The numerical results presented in this work do not make any such assumption.)

Non-standard neutrino interactions can affect the production and detection of neutrinos at the source and detector, respectively. In the SM, interactions of charged leptons with neutrinos are strictly flavour-diagonal. However, charged-current NSIs can introduce a non-zero overlap between charged leptons and neutrinos of different flavours. Thus, a neutrino produced at a source in association with a charged lepton ℓ_α is not simply ν_α , but is given by [20, 28–30]

$$|\nu_\alpha^s\rangle = |\nu_\alpha\rangle + \sum_{\gamma=e,\mu,\tau} \varepsilon_{\alpha\gamma}^s |\nu_\gamma\rangle. \quad (8)$$

Similarly, a neutrino that produces a charged lepton ℓ_β in a detector is

$$\langle \nu_\beta^d | = \langle \nu_\beta | + \sum_{\gamma=e,\mu,\tau} \varepsilon_{\gamma\beta}^d \langle \nu_\gamma |. \quad (9)$$

The matrices ε^s and ε^d are in general complex, giving 36 new parameters. These are 9 amplitudes and 9 phases of each NSI parameter in the source and detector NSI matrices.

Not all of the 36 NSI parameters are relevant for the experiment under consideration. Since we are only interested in the oscillation channels $\nu_\mu \rightarrow \nu_e$ and $\nu_\mu \rightarrow \nu_\mu$ (and their CP

conjugates), the relevant parameters are $\varepsilon_{\mu\gamma}^s$, $\varepsilon_{\gamma e}^d$ and $\varepsilon_{\gamma\mu}^d$, where $\gamma \in \{e, \mu, \tau\}$. Thus, the parameter space is reduced to 9 complex or 18 real parameters, in addition to the standard ones. In this work, we treat all of them as independent parameters, which is the most general case.

Deriving an analytical formula for the neutrino oscillation probabilities is difficult even in the standard three-flavour scenario. Typically, expressions for the probabilities are given as perturbative expansions in small parameters such as $\Delta m_{21}^2/\Delta m_{31}^2$ or $\sin \theta_{13}$ [31–33]. For the discussion in this section, we refer to the analytical formulae for vacuum oscillation probabilities derived in Ref. [34], which include source and detector NSIs. These formulae are valid up to second order in $\Delta m_{21}^2/\Delta m_{31}^2$ and $\sin \theta_{13}$, and up to first order in the NSI parameters. It is easy to observe that linearizing the expressions in the NSI parameters and ignoring cubic and higher order terms overall, leaves only a few NSI parameters in the expressions. For instance, in the case of the vacuum probability $P_{\mu e}$, only the NSI parameters $\varepsilon_{\mu e}^s$, $\varepsilon_{\mu e}^d$ and $\varepsilon_{\tau e}^d$ are present up to linear order. While these approximate analytical formulae provide useful insights into the physics of NSIs in neutrino oscillations, we stress that all simulation results presented in this work make use of numerically computed neutrino oscillation probabilities without approximations.

In Fig. 1, we have plotted the variation of the neutrino oscillation probability $P_{\mu e}$ with the amplitude of each of the relevant NSI parameters. The range of values chosen for the NSI parameters is the 90% C.L. bounds on them as listed in Eq. (7). Each of the probabilities shown are calculated numerically, using $\delta = 0$, $\theta_{23} = 45^\circ$ and normal neutrino mass ordering; and all other NSI parameters, including phases, set to zero. Out of the three NSI parameters present up to linear order, the variation due to $\varepsilon_{\tau e}^d$ is the strongest, while that due to $\varepsilon_{\mu e}^d$ is the weakest. This pattern follows from the allowed range given by the current bounds. Out of the remaining three, $\varepsilon_{\mu\mu}^s$ has the greatest effect, which is again because it is not very tightly constrained by current data.

Figure 1 is plotted for a fixed value of $\delta = 0$. For ESS ν SB, it is interesting to explore the interplay between δ and the NSI parameters. To this end, we show in Fig. 2 bi-probability plots for ESS ν SB. This figure is presented for a fixed energy of 400 MeV, which corresponds to the second oscillation maximum for the ESS ν SB baseline. This is also the energy around which the unoscillated event rate is maximal. As δ varies over its full range, the neutrino and antineutrino probabilities trace out an ellipse as shown. In the standard case, we obtain

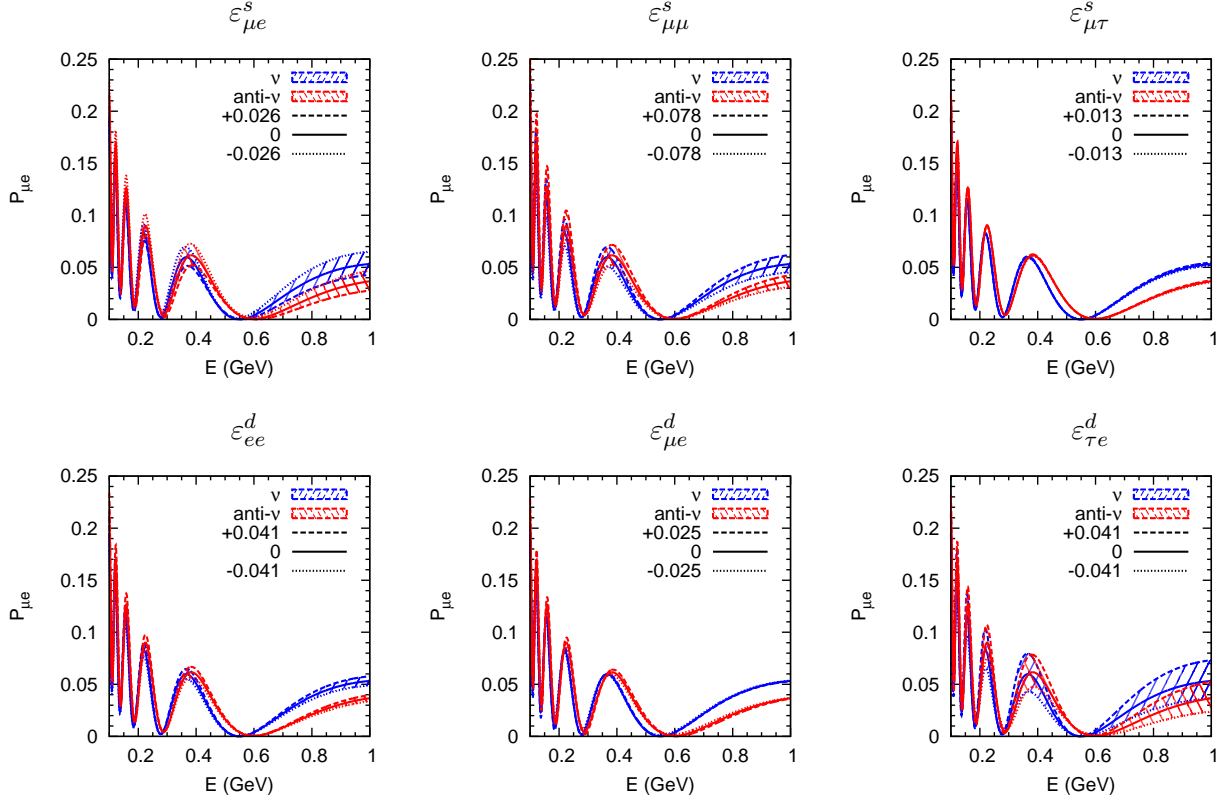


FIG. 1. Neutrino oscillation probability $P_{\mu e}$ as a function of the neutrino energy E and its variation with each of the relevant NSI parameters. The values of the NSI parameters are chosen within their 90% C.L. bounds, i.e. assuming their phases to be either 0 or π . The variation is shown for both neutrinos and antineutrinos. The values of the fundamental neutrino parameters are set to $\Delta m_{21}^2 = 7.6 \times 10^{-5} \text{ eV}^2$, $\Delta m_{31}^2 = 2.45 \times 10^{-3} \text{ eV}^2$, $\sin^2 \theta_{12} = 0.304$, $\theta_{23} = 45^\circ$, $\sin^2 2\theta_{13} = 0.09$ and $\delta = 0$.

the central (blue) ellipse. In each of the panels of this figure, one NSI parameter is varied within its 90% C.L. bound, which gives the spread in the ellipse.

In order to explain the features observed in Fig. 2, we define the variation of the neutrino oscillation probability as

$$\Delta P_{\mu e}^{\text{vac}}(\varepsilon_{\alpha\beta}^x) = P_{\mu e}^{\text{vac}}(\varepsilon_{\alpha\beta}^x) - P_{\mu e}^{\text{vac}}(\varepsilon_{\alpha\beta}^x = 0) , \quad (10)$$

where $\alpha, \beta \in \{e, \mu, \tau\}$ and $x \in \{s, d\}$. Using the perturbative analytical expression for $P_{\mu e}^{\text{vac}}$

from Ref. [34], we obtain for the cases of $\varepsilon_{\mu e}^s$, $\varepsilon_{\mu e}^d$ and $\varepsilon_{\mu\tau}^d$

$$\Delta P_{\mu e}^{\text{vac}}(\varepsilon_{\mu e}^s) \simeq -4|\varepsilon_{\mu e}^s| \sin \theta_{13} \sin \theta_{23} \sin(\Delta + \delta) \sin \Delta, \quad (11)$$

$$\begin{aligned} \Delta P_{\mu e}^{\text{vac}}(\varepsilon_{\mu e}^d) &\simeq -4|\varepsilon_{\mu e}^d| \sin \theta_{13} \cos 2\theta_{23} \sin \theta_{23} \cos \delta \sin^2 \Delta \\ &\quad -2|\varepsilon_{\mu e}^d| \sin \theta_{13} \sin \theta_{23} \sin \delta \sin 2\Delta \\ &\quad + |\varepsilon_{\mu e}^d| \frac{\Delta m_{21}^2}{\Delta m_{31}^2} \Delta \sin 2\theta_{12} \sin 2\theta_{23} \sin \theta_{23} \sin 2\Delta, \end{aligned} \quad (12)$$

$$\begin{aligned} \Delta P_{\mu e}^{\text{vac}}(\varepsilon_{\tau e}^d) &\simeq 4|\varepsilon_{\tau e}^d| \sin \theta_{13} \sin 2\theta_{23} \sin \theta_{23} \cos \delta \sin^2 \Delta \\ &\quad + |\varepsilon_{\tau e}^d| \frac{\Delta m_{21}^2}{\Delta m_{31}^2} \Delta \sin 2\theta_{12} \sin 2\theta_{23} \cos \theta_{23} \sin 2\Delta, \end{aligned} \quad (13)$$

where $\Delta \equiv \Delta m_{31}^2 L / (4E)$. In deriving each of Eqs. (11)-(13), we have set all other NSI parameters to zero. Note that for the cases of $\varepsilon_{\mu\mu}^s$, $\varepsilon_{\mu\tau}^s$ and ε_{ee}^d , there are no linear-order terms in the corresponding formulae, and the dependence on the NSI parameters only appear at second order and above. First, we observe (as in Fig. 1) that the variation of $P_{\mu e}$ is the largest for $\varepsilon_{\tau e}^d$ (due to linear variation and weakest upper bound) and the smallest for $\varepsilon_{\mu\tau}^s$ (due to higher-order variation and strongest upper bound). For $\varepsilon_{\mu e}^s$, $\varepsilon_{\mu\mu}^s$, ε_{ee}^d and $\varepsilon_{\mu e}^d$, the variations are intermediate, depending on a non-trivial combination between the value of the upper bound on the considered NSI parameter and if this NSI parameter appears at linear order or not in the variation. Second, we can explain the structure of the band for each panel. We illustrate this for the case of $\varepsilon_{\mu e}^s$. For the baseline and energy considered, Δ evaluates to around -120° , close to the second oscillation maximum. It is then easy to see that the maximum ‘width’ of the band occurs when $\Delta + \delta = \pm 90^\circ$, i.e. when δ is around 30° or -150° . Likewise, for $\Delta + \delta = 0, 180^\circ$, the probability becomes independent of $\varepsilon_{\mu e}^s$, and the band ‘pinches off’. This occurs when δ is around 120° or -60° . For antineutrinos, the sign of δ is changed, and one can use similar arguments to find the broadest and narrowest points along the $\overline{P_{\mu e}}$ axis as well.

Finally, Fig. 3 shows the neutrino and antineutrino event rates for ESS ν SB in a bi-rate plot, using the same parameter values as for Fig. 2. The event rates plotted are the total rates across all energy bins. Statistical error bars have been included for four representative values of δ . In addition to the variation of the probabilities in Fig. 2, this figure gives a first indication of the impact of NSIs versus the possible experimental resolution of the ESS ν SB. Where the experimental error bars on the total event rates are smaller than the possible variation of the NSI parameters, the ESS ν SB will generally be sensitive to NSIs smaller

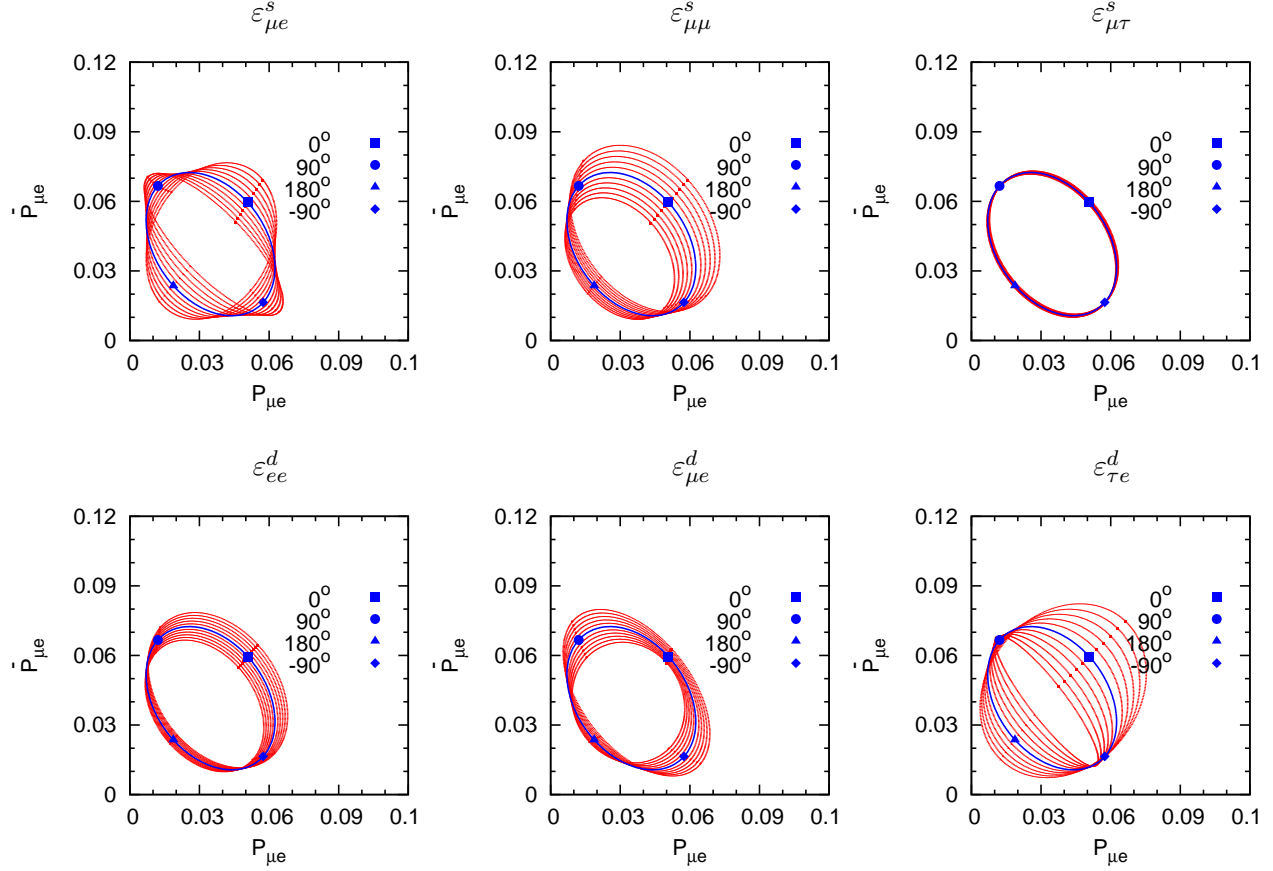


FIG. 2. Bi-probability ellipse for ESSνSB and its variation with the relevant NSI parameters. The values of the fundamental neutrino parameters and the NSI parameters are the same as in Fig. 1.

than the current bounds. However, note that the converse is not necessarily true as the experimental results do not only include the total event rates, but also spectral information, which may also be used to constrain the NSIs. In particular, this will be apparent for our results on $\varepsilon_{\mu e}^d$, which does not change the event rates significantly.

V. RESULTS ON NSIS AT ESSνSB

The main goal of the proposed ESSνSB experiment is to measure the CP-violating phase δ with high precision. In this section, we examine both the impact of the NSI parameters on this δ measurement and the ability of ESSνSB to measure the NSI parameters.

The central values of the neutrino parameters Δm_{21}^2 , $|\Delta m_{31}^2|$, θ_{12} and θ_{13} are taken close to their current best-fit values [6–8]. We have also imposed Gaussian priors on these parameters with a width obtained from these global fits. The values of θ_{23} and δ used are different in

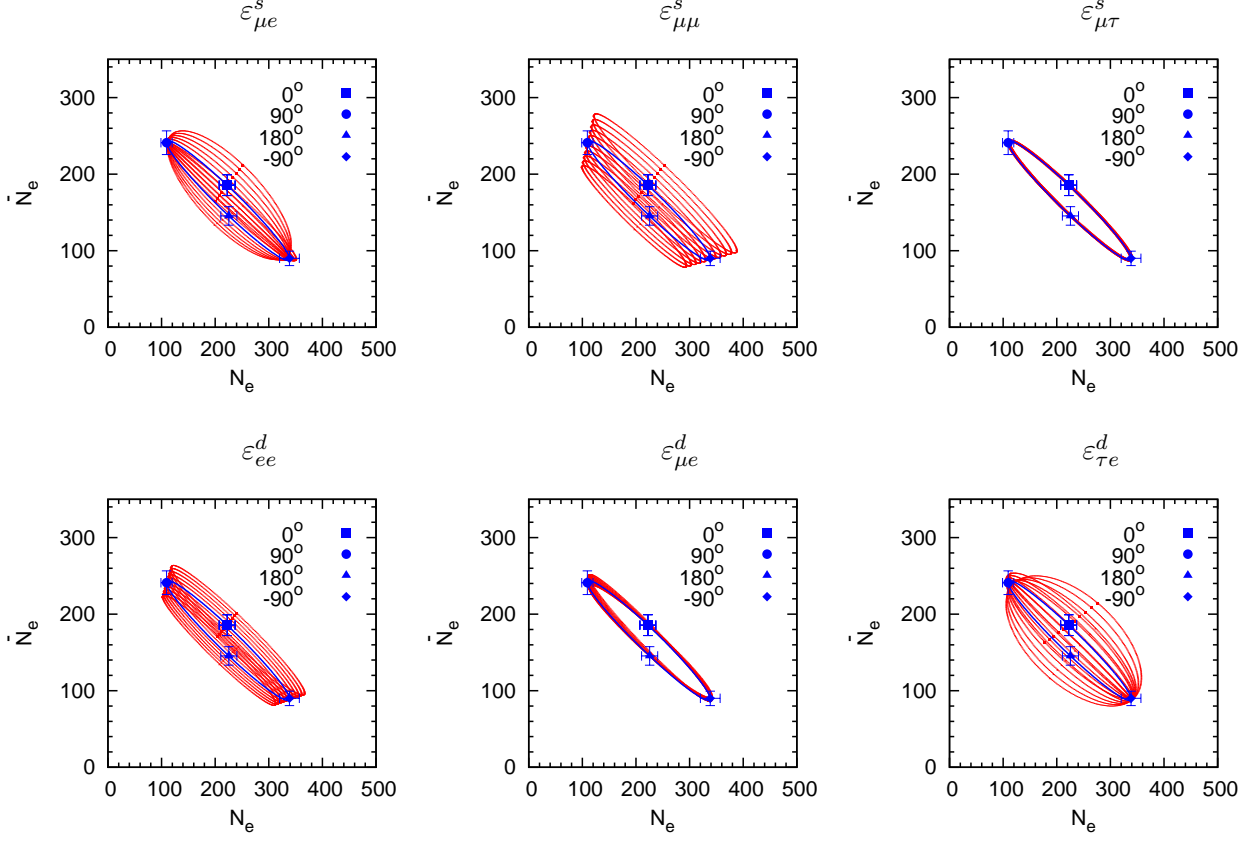


FIG. 3. Bi-rates ellipse for ESSνSB and its variation with the relevant NSI parameters. The values of the fundamental neutrino parameters and the NSI parameters are the same as in Fig. 1.

each case, and are specified in the text. In addition, we have assumed a 5% prior on the true value of $\sin^2 2\theta_{23}$. The NSI parameters are of the form $\varepsilon_{\alpha\beta}^x$, where $\alpha, \beta \in \{e, \mu, \tau\}$ and $x \in \{s, d\}$, since the source and detector NSI parameters can be different in general. Thus, we have 18 complex NSI parameters, or 36 real NSI parameters, in addition to the standard ones. We have run our simulations for both normal (NO) and inverted (IO) neutrino mass ordering. We find that there is very little qualitative difference between the results in these two cases. Therefore, in what follows, we show only the NO results.

A. Effect on precision measurement at ESSνSB

In this subsection, we discuss the interplay between NSI parameters and the δ precision of ESSνSB. The results are shown in the form of precision contours in the $\theta_{23}-\delta$ plane. This is performed for three representative values of $\theta_{23} \in \{42^\circ, 45^\circ, 48^\circ\}$; and four representative

values of $\delta \in \{-90^\circ, 0^\circ, 90^\circ, 180^\circ\}$.

First, we explore the effect of marginalizing over the source and detector NSI parameters on precision measurements at ESS ν SB, in the special case the true NSI parameters are zero. In other words, we take all the NSI parameters to be zero when generating the mock data, but allow them all to vary in the fit. Thus, these plots show the robustness of the ESS ν SB measurements against a scan for NSIs. The results are shown in Fig. 4. The solid curves show the 68%, 90% and 95% C.L. contours for the allowed region in the parameter space. The dashed contours are for the standard case where there are no NSI parameters in the data or the fit.

We observe that the search for NSIs does not affect the θ_{23} precision of ESS ν SB much. The precision in δ is worsened to at most twice its standard precision, in the worst case. For most cases, the precision is seen to be quite robust, even in spite of a severely enlarged parameter space. This is true, irrespective of the true value of θ_{23} or δ .

Second, in Fig. 5, we investigate the same effect as in Fig. 4, but with a non-zero value for the NSI parameters in the mock data. These ‘true’ values of the NSI parameters have been taken to be half of the bounds given in Eq. (7) for the amplitudes. The true values of the non-standard phases are taken to be zero. In the fit, as before, all the standard as well as the NSI parameters are marginalized over. Thus, these plots show the robustness of measurements at ESS ν SB against a scan for NSI parameters, but in the presence of NSIs.

As in the previous case, in the presence of NSIs, we observe that the θ_{23} measurement is not affected much, while the precision in δ worsens. Here, the worsening depends significantly on the value of δ in nature. When $\delta = 0$, the worsening of precision is least, whereas for $\delta = 180^\circ$, the precision is worst. This is seen uniformly across the range of θ_{23} values considered. The reason for this is as follows. A measure of the precision of δ is $dP_{\mu e}^{\text{vac}}/d\delta$. In order to find the value of δ at which this precision is minimal, we set the derivative of this quantity, i.e. $d^2P_{\mu e}^{\text{vac}}/d\delta^2$ to zero. Since the dependence of the probability on δ is harmonic, the second derivative is proportional to the probability itself. As seen from the panels in Fig. 2, the smallest probability for both neutrinos and antineutrinos is around 180° . This is why the precision of δ is worst at 180° in the presence of NSIs.

Third, we study how the precision measurement at ESS ν SB would be affected if NSIs are present in nature, but are not accounted for in the scan of the parameter space. For this, we have taken non-zero values of the NSI parameters in the mock data (the same non-zero

values as in the previous case of Fig. 5), but their values have been kept fixed at zero in the fit. The results are displayed in Fig. 6. Here, the solid curves represent the 68%, 90% and 95% C.L. contours, when NSIs are present in the data, but not in the fit. The dashed curves are the corresponding contours for the case where the NSIs are marginalized over in the fit. Thus, the difference between the solid and dashed contours indicates the effect of our ignorance of the existence of NSIs. Our ignorance leads us to an over-optimistic precision in δ , as expected. The effect is more pronounced for the true value of $\delta = 180^\circ$. As before, the θ_{23} precision is not affected.

B. Constraining NSI parameters at ESS

Having investigated the effect of NSIs on precision measurements at ESS ν SB, we explore the ability of this experiment to measure the NSI parameters themselves. As we have seen before, the effect of the NSI parameters on the probability is quite mild. Therefore, we do not expect to obtain very strong constraints on these parameters.

Figure 7 shows the limits which ESS ν SB can set on the amplitudes of the NSI parameters for NO, $\theta_{23} = 45^\circ$ and $\delta = 0$. Consider the top-left panel, corresponding to the parameter $\varepsilon_{\mu e}^s$. In generating this plot, we have set the true values of the NSI parameters to be zero. We show the χ^2 as a function of the test value of $|\varepsilon_{\mu e}^s|$, when all the other neutrino parameters, including the NSI ones are marginalized over. Horizontal lines have been drawn in the plots, corresponding to 68%, 90% and 95% C.L., assuming a χ^2 distribution. One can read off the limits that ESS ν SB can impose on these parameters from this plot. Similarly, the other panels show the limits for the other relevant parameters.

The 90% C.L. limits on the NSI parameters using data from ESS ν SB are summarized in Table I. The first column gives the limits when all the other NSI parameters are kept free in the fit, which can be simply read off from Fig. 7. These limits should be interpreted as being realistic, since they are derived without making any assumptions on the values of the other NSI parameters. We have also computed the limits when the NSI parameters are only considered one at a time, i.e. all other NSI parameters are fixed to zero. These limits, which are given in the second column, are more optimistic. The realistic limits on $|\varepsilon_{\mu e}^s|$ and $|\varepsilon_{\mu e}^d|$ are comparable to the ones in Ref. [21], which are listed in the third column for ease

of comparison.² This is because these parameters have the maximum effect on $P_{\mu e}$, as seen from the analytical expressions. In the optimistic case, the limits on $|\varepsilon_{\mu e}^s|$ and $|\varepsilon_{\mu e}^d|$ improve by a factor of two compared to the existing bounds. For all the other NSI parameters (except $|\varepsilon_{\mu e}^s|$ and $|\varepsilon_{\mu e}^d|$), the realistic and optimistic limits basically coincide and are less stringent than the limits in Ref. [21].

Parameter	Limits with all other	Limits with all other	Limits from Ref. [21]
	NSI parameters free	NSI parameters zero	
$ \varepsilon_{\mu e}^s $	0.025	0.014	0.026
$ \varepsilon_{\mu\mu}^s $	0.27	0.27	0.078
$ \varepsilon_{\mu\tau}^s $	0.040	0.040	0.013
$ \varepsilon_{ee}^d $	0.15	0.15	0.041
$ \varepsilon_{e\mu}^d $	0.087	0.082	0.026
$ \varepsilon_{\mu e}^d $	0.025	0.014	0.025
$ \varepsilon_{\mu\mu}^d $	0.28	0.27	0.078
$ \varepsilon_{\tau e}^d $	0.11	0.12	0.041
$ \varepsilon_{\tau\mu}^d $	0.040	0.033	0.013

TABLE I. 90% C.L. sensitivities of ESS ν SB to the NSI parameters.

We have also checked whether ESS ν SB can measure the values of the NSI parameters with any reasonable precision. The procedure for this is the same as for Fig. 7, except that the true values of the NSI parameters are non-zero. We have chosen these true values to be half of the 90% C.L. bounds given in Ref. [21]. The χ^2 resulting from these computations is shown in Figs. 8 and 9 for the amplitudes and the phases of the NSI parameters, respectively. We find that ESS ν SB is not capable of distinguishing the chosen non-zero values of the parameters from zero, even at 68% C.L., nor is it able to significantly constrain any of the NSI phases.

² Note that the limit on a given NSI parameter in Ref. [21] has been computed considering only that parameter and assuming all other NSI parameters to be zero, which corresponds to the optimistic case.

C. Role of near detector and systematics

Throughout this study we have used systematic errors of 9% in the signal and 18% in the background events [24]. These are typical values for a superbeam experiment with a megaton-scale water Cherenkov detector. In order to study the role of systematic errors on our results, we have also simulated our experiment with a smaller systematic error of 5% in both signal and background. This is of course a very optimistic value. We have found that the limits on NSIs from ESS ν SB do not change appreciably with this drastic reduction of systematic errors. This is because in spite of having a large detector and intense source, ESS ν SB is still statistics-dominated due to the lower event rate at the second oscillation maximum.

Finally, we examine the role played by the near detector in the sensitivity of ESS ν SB. As described before, we have used a crude simulation of the near detector throughout this work. Here, we compare the results of our simulation with and without the near detector. We show in Fig. 10 a recomputed version of Fig. 5, both with and without the near detector. The solid contours are the same as before, but the dashed contours show the same allowed regions, if only the far detector is used. We observe that in the absence of a near detector, the δ -sensitivity of ESS ν SB is worsened. The limits on NSI parameters are also worse without the near detector.

VI. SUMMARY AND CONCLUSIONS

In this work, we have investigated the effects of source and detector NSIs at the proposed neutrino oscillation experiment ESS ν SB, with a baseline of 540 km – the source being the ESS in Lund, Sweden and a MEMPHYS-like detector in Garpenberg, Sweden. The ESS ν SB experiment is designed to determine the leptonic CP-violating phase δ at the second oscillation maximum. However, it may also be able to probe source and detector NSIs. Due to the short baseline length and low neutrino energy of this experiment, matter NSIs will not be of importance, and are therefore not considered in this work.

First, we have studied the three-flavour neutrino oscillation probabilities with source and detector NSIs, which depend on six relevant NSI parameters – $\varepsilon_{\mu e}^s$, $\varepsilon_{\mu\mu}^s$, $\varepsilon_{\mu\tau}^s$, ε_{ee}^d , $\varepsilon_{\mu e}^d$ and $\varepsilon_{\tau e}^d$. We used perturbative analytical expressions for the $\nu_\mu \rightarrow \nu_e$ channel that is the important

channel for ESS ν SB in which $\varepsilon_{\mu e}^s$, $\varepsilon_{\mu e}^d$ and $\varepsilon_{\tau e}^d$ are the dominating NSI parameters in order to observe the impact of these parameters. We have found that, for the range of values allowed by the current data, the NSI parameter $\varepsilon_{\tau e}^d$ affect this probability the most, whereas the NSI parameter $\varepsilon_{\mu e}^d$ the least. All other four NSI parameters have intermediate influence on the probability.

Second, we have explored the effect of marginalizing over the NSI parameters on precision measurements at ESS ν SB using two cases: (i) The true values of the NSI parameters are set to zero and (ii) the true values are set to half of the current 90% C.L. bounds. In both cases, the precision of measuring δ is reduced by at most a factor of two. In addition, a measurement of the leptonic mixing angle θ_{23} is not affected by NSIs. If we do not take the effect of NSIs into account when determining the value of δ , we obtain over-optimistic results. The effect is most pronounced for a true value of $\delta = 180^\circ$. Note that the impact of NSIs on the results are qualitatively same for both NO and IO.

Third, we have determined the possibility of ESS ν SB to measure the values of the NSI parameters. In a realistic case with all NSI parameters free, we have found limits on $\varepsilon_{\mu e}^s$ and $\varepsilon_{\mu e}^d$ at 90% C.L. that are similar to the existing limits in the literature, whereas in a optimistic case with only one NSI parameter free and the rest set to zero, the limits on $\varepsilon_{\mu e}^s$ and $\varepsilon_{\mu e}^d$ are improved by a factor of two. Furthermore, we have set the true values of the NSI parameters to half of their existing bound, and found that ESS ν SB is not able to differentiate the set values from zero at 68% C.L. or impose any significant constraints on the phases of the NSI parameters.

Finally, we have examined the influence of the presence of a near detector at the ESS ν SB experimental setup. Indeed, we show that without a near detector the results would be more pessimistic concerning both the sensitivity of δ and the limits on the NSI parameters. Note that the results are not changed significantly by reducing the systematic errors.

In conclusion, using ESS ν SB with a near detector, the presence of NSIs will at most reduce the measurement of δ by a factor of two, while a measurement of θ_{23} will remain robust. In addition, it is possible to improve the existing upper limits on some of the NSI parameters by a factors of two.

ACKNOWLEDGMENTS

This work was supported by the Göran Gustafsson Foundation (M.B.). S.C. acknowledges support from the Neutrino Project under the XII plan of Harish-Chandra Research Institute and partial support from the European Union FP7 ITN INVISIBLES (Marie Curie Actions, PITN-GA-2011-289442). We thank Pilar Coloma, Michal Malinský, Suprabh Prakash, Bedřich Roskovec and Nikos Vassilopoulos for useful discussions.

-
- [1] G. Aad et al. (ATLAS), Phys. Lett. **B716**, 1 (2012), 1207.7214.
 - [2] S. Chatrchyan et al. (CMS), Phys. Lett. **B716**, 30 (2012), 1207.7235.
 - [3] S. Weinberg, Phys. Rev. Lett. **43**, 1566 (1979).
 - [4] J. Davis, Raymond, D. S. Harmer, and K. C. Hoffman, Phys. Rev. Lett. **20**, 1205 (1968).
 - [5] Y. Fukuda et al. (Super-Kamiokande), Phys. Rev. Lett. **81**, 1562 (1998), hep-ex/9807003.
 - [6] F. Capozzi, G. Fogli, E. Lisi, A. Marrone, D. Montanino, et al., Phys. Rev. **D89**, 093018 (2014), 1312.2878.
 - [7] D. Forero, M. Tortola, and J. Valle, Phys. Rev. **D90**, 093006 (2014), 1405.7540.
 - [8] M. Gonzalez-Garcia, M. Maltoni, and T. Schwetz, JHEP **11**, 052 (2014), 1409.5439.
 - [9] E. Baussan et al. (ESSnuSB), Nucl. Phys. **B885**, 127 (2014), 1309.7022.
 - [10] S. K. Agarwalla, S. Choubey, and S. Prakash, JHEP **12**, 020 (2014), 1406.2219.
 - [11] M. Blennow, P. Coloma, and E. Fernandez-Martinez, JHEP **12**, 120 (2014), 1407.1317.
 - [12] T. Ohlsson, Rept. Prog. Phys. **76**, 044201 (2013), 1209.2710.
 - [13] O. Miranda and H. Nunokawa (2015), 1505.06254.
 - [14] S. Antusch, J. P. Baumann, and E. Fernandez-Martinez, Nucl. Phys. **B810**, 369 (2009), 0807.1003.
 - [15] C. Biggio, M. Blennow, and E. Fernandez-Martinez, JHEP **03**, 139 (2009), 0902.0607.
 - [16] L. Wolfenstein, Phys. Rev. **D17**, 2369 (1978).
 - [17] V. D. Barger, R. Phillips, and K. Whisnant, Phys. Rev. **D44**, 1629 (1991).
 - [18] S. Mikheyev and A. Y. Smirnov, Sov. J. Nucl. Phys. **42**, 913 (1985).
 - [19] S. Mikheyev and A. Y. Smirnov, Nuovo Cim. **C9**, 17 (1986).
 - [20] Y. Grossman, Phys. Lett. **B359**, 141 (1995), hep-ph/9507344.

- [21] C. Biggio, M. Blennow, and E. Fernandez-Martinez, JHEP **08**, 090 (2009), 0907.0097.
- [22] T. Ohlsson and H. Zhang, Phys. Lett. **B671**, 99 (2009), 0809.4835.
- [23] S. K. Agarwalla, P. Bagchi, D. V. Forero, and M. Tórtola, JHEP **07**, 060 (2015), 1412.1064.
- [24] L. Agostino et al. (MEMPHYS), JCAP **01**, 024 (2013), 1206.6665.
- [25] P. Huber, M. Lindner, and W. Winter, Comput. Phys. Commun. **167**, 195 (2005), hep-ph/0407333.
- [26] P. Huber, J. Kopp, M. Lindner, M. Rolinec, and W. Winter, Comput. Phys. Commun. **177**, 432 (2007), hep-ph/0701187.
- [27] M. Blennow and E. Fernandez-Martinez, Comput. Phys. Commun. **181**, 227 (2010), 0903.3985.
- [28] M. Gonzalez-Garcia, Y. Grossman, A. Gusso, and Y. Nir, Phys. Rev. **D64**, 096006 (2001), hep-ph/0105159.
- [29] S. M. Bilenky and C. Giunti, Phys. Lett. **B300**, 137 (1993), hep-ph/9211269.
- [30] D. Meloni, T. Ohlsson, W. Winter, and H. Zhang, JHEP **04**, 041 (2010), 0912.2735.
- [31] A. Cervera, A. Donini, M. Gavela, J. Gomez Cadenas, P. Hernandez, et al., Nucl. Phys. **B579**, 17 (2000), hep-ph/0002108.
- [32] M. Freund, Phys. Rev. **D64**, 053003 (2001), hep-ph/0103300.
- [33] E. K. Akhmedov, R. Johansson, M. Lindner, T. Ohlsson, and T. Schwetz, JHEP **04**, 078 (2004), hep-ph/0402175.
- [34] J. Kopp, M. Lindner, T. Ota, and J. Sato, Phys. Rev. **D77**, 013007 (2008), 0708.0152.

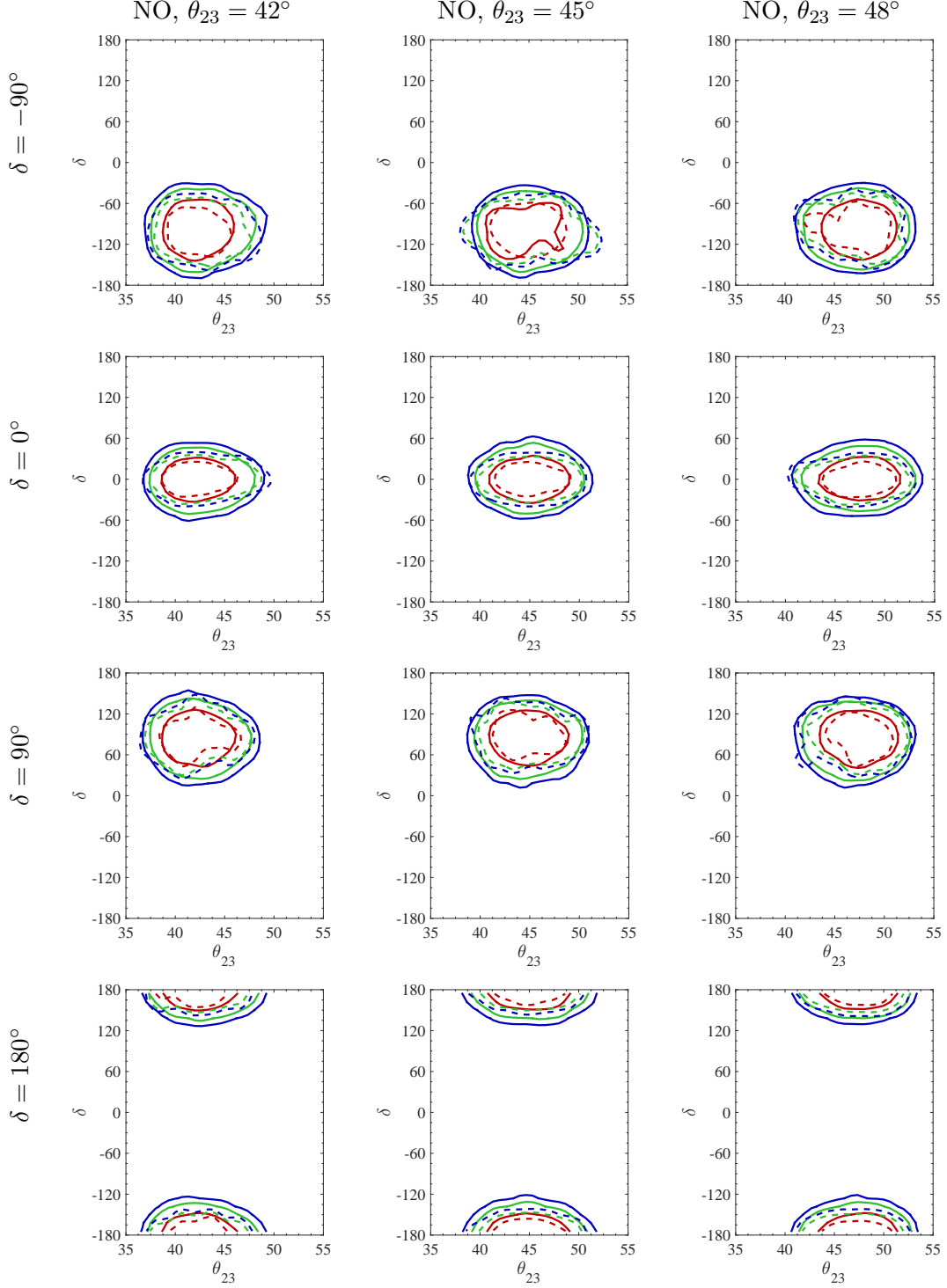


FIG. 4. Effect of marginalizing over source and detector NSI parameters on precision measurements at ESSνSB. Each panel shows the allowed region in the test $\theta_{23} - \delta$ plane, when the NSI parameters are taken to be zero in the data. The red, green and blue curves represent the 68%, 90% and 95% C.L. contours, respectively. The solid contours show the effect of marginalization over the NSI parameters, whereas the dashed contours are for the standard oscillation scenario in the absence of NSIs.

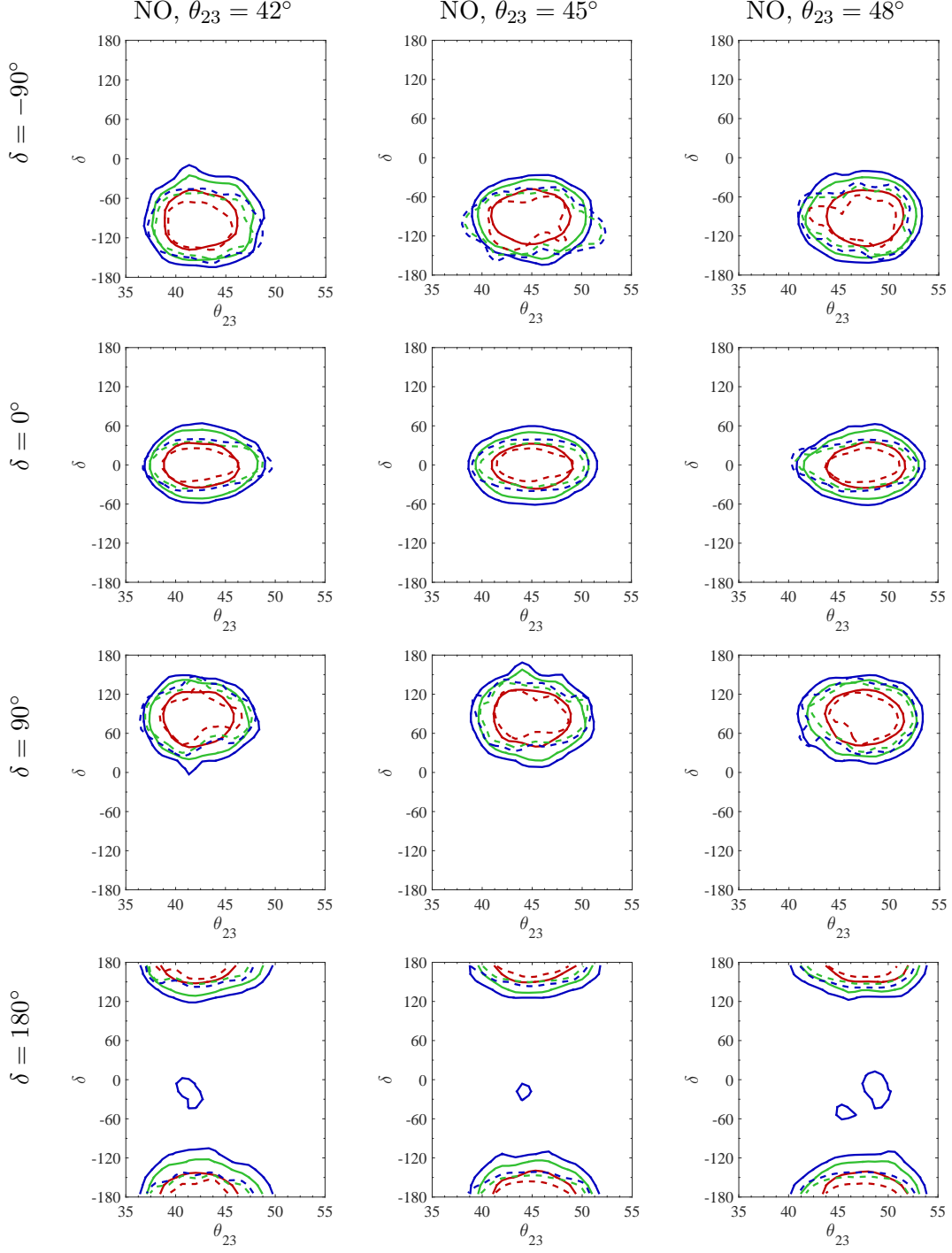


FIG. 5. Effect of marginalizing over source and detector NSI parameters on precision measurements at ESSνSB. Each panel shows the allowed region in the test $\theta_{23} - \delta$ plane, when the NSI parameters are taken to be non-zero in the data. The true values of the amplitudes of the NSI parameters are assumed to be half of their 90% C.L. bounds from Ref. [21]. The red, green and blue curves represent the 68%, 90% and 95% C.L. contours, respectively. The solid contours show the effect of marginalization over the NSI parameters, whereas the dashed contours are for the standard oscillation scenario in the absence of NSIs.

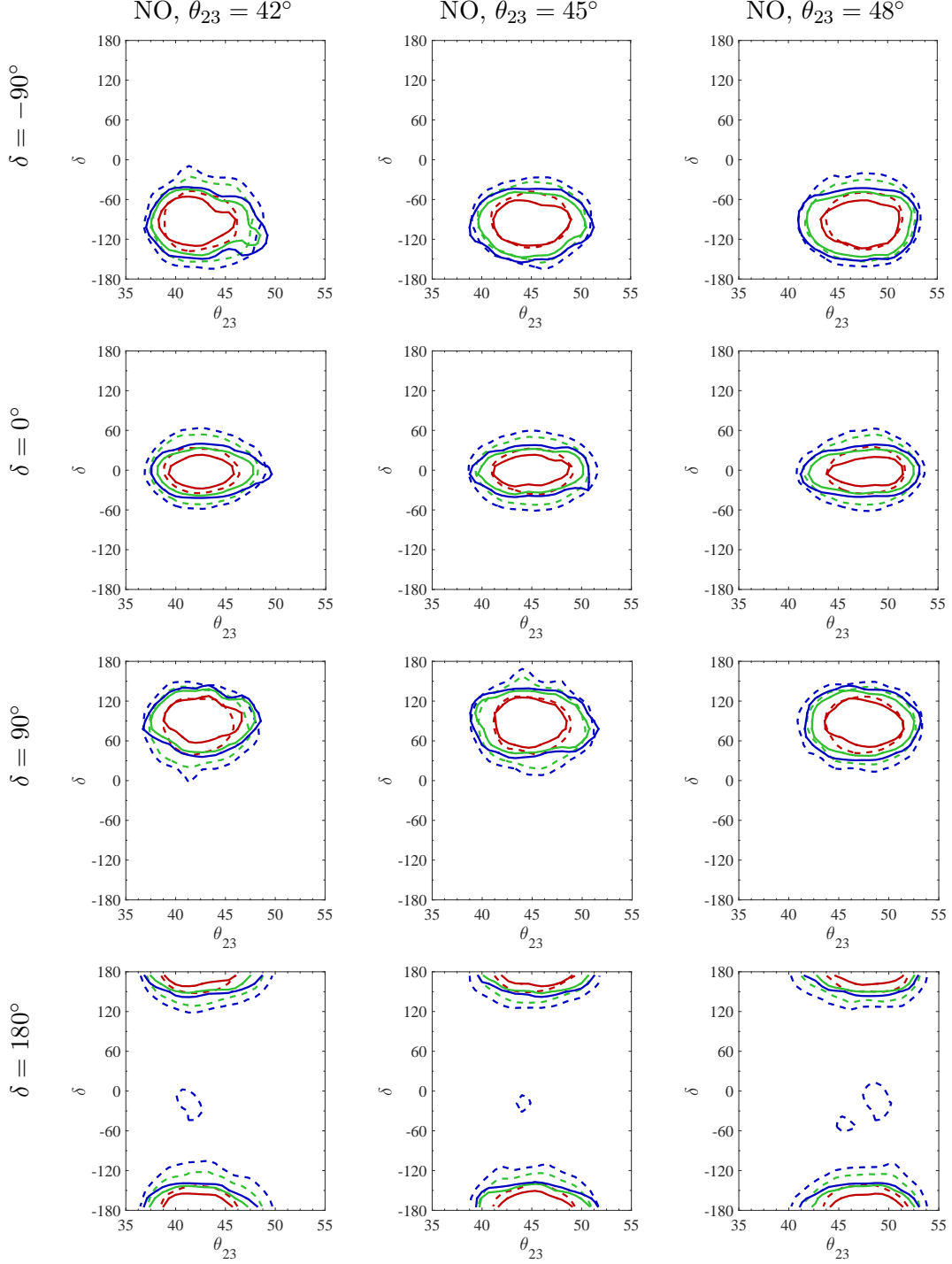


FIG. 6. Precision measurements at ESSνSB for the case where NSIs are present in nature, but are not scanned for. Each panel shows the allowed region in the test $\theta_{23} - \delta$ plane, when the NSI parameters are taken to be non-zero in the data. The true values of the amplitudes of the NSI parameters are assumed to be half of their 90% C.L. bounds from Ref. [21]. The red, green and blue curves represent the 68%, 90% and 95% C.L. contours, respectively. The solid (dashed) contours show the allowed region without (with) marginalization over the NSI parameters.

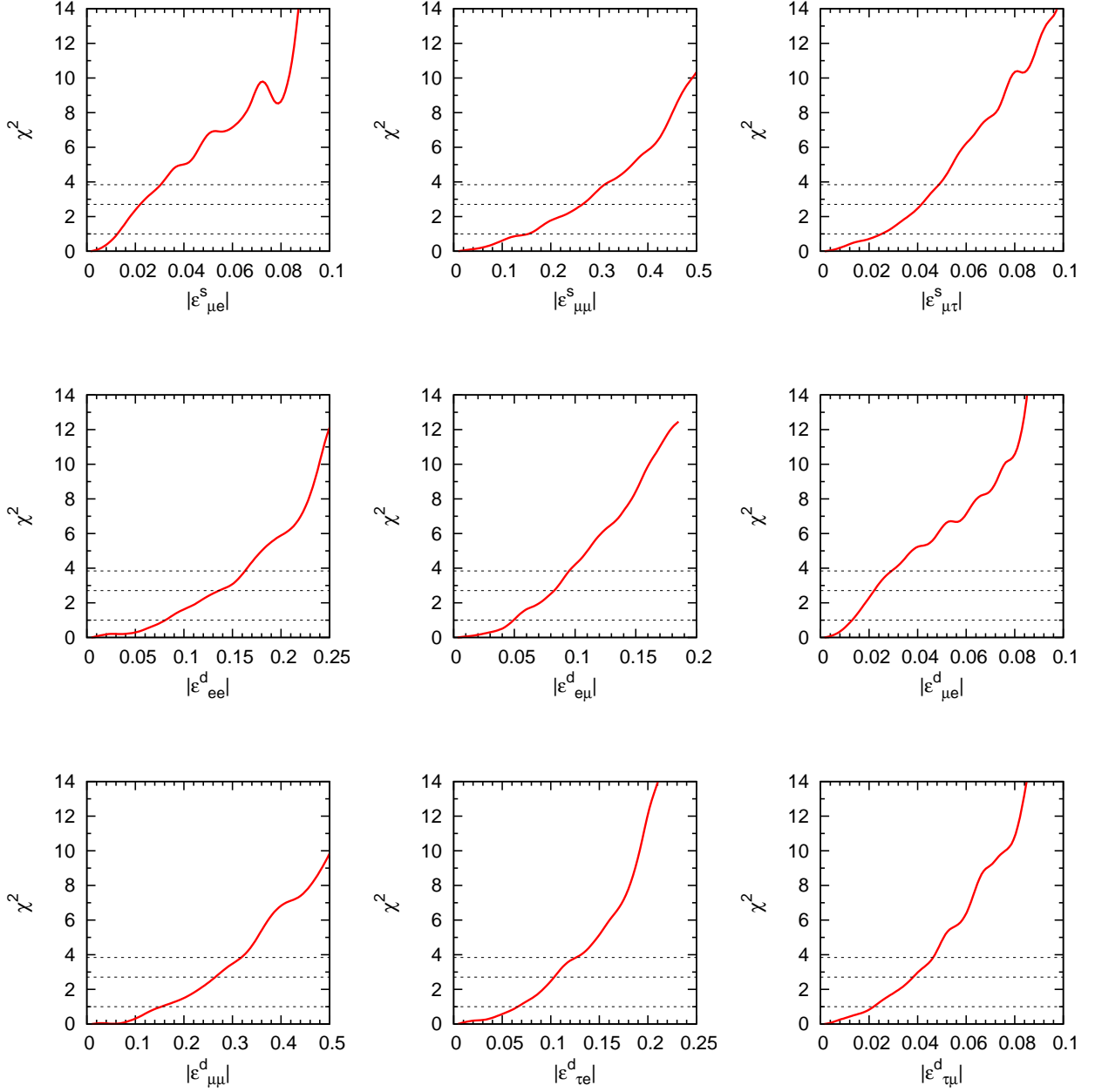


FIG. 7. Limits on the amplitudes of the NSI parameters imposed by ESS ν SB data: χ^2 as a function of the test value of the amplitudes of the NSI parameters, when the true value is zero. In each panel, all neutrino parameters (apart from the one indicated) have been marginalized over. The dotted lines from bottom to top show the 68%, 90% and 95% C.L., respectively.

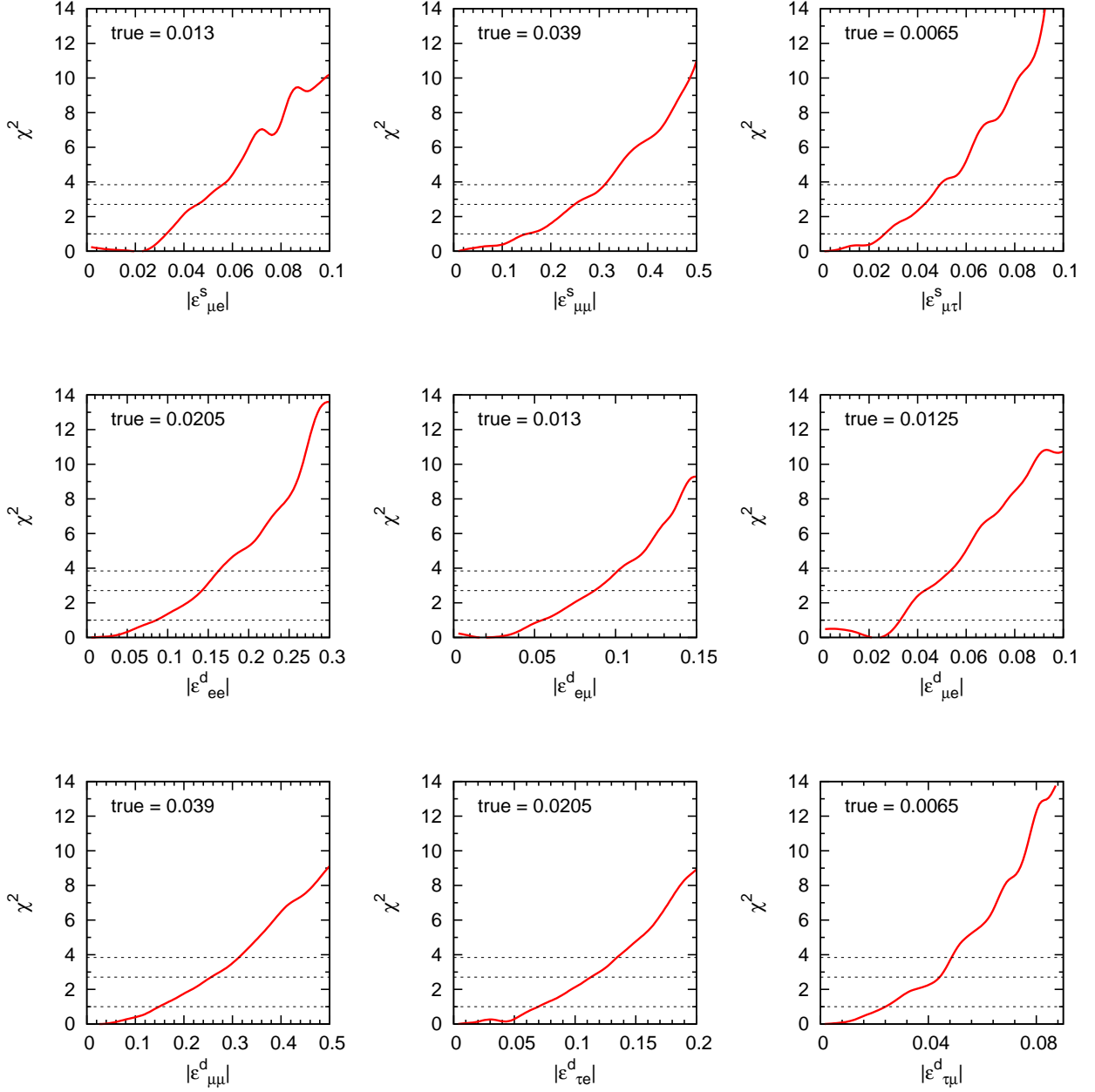


FIG. 8. Precision on the amplitudes of the NSI parameters from ESSνSB data: χ^2 as a function of the test value of the amplitudes of the NSI parameters, when the true value is non-zero. The true values of the amplitudes of the NSI parameters are assumed to be half of their 90% C.L. bounds from Ref. [21]. In each panel, all neutrino parameters (apart from the one indicated) have been marginalized over. The dotted lines from bottom to top show the 68%, 90% and 95% C.L., respectively.

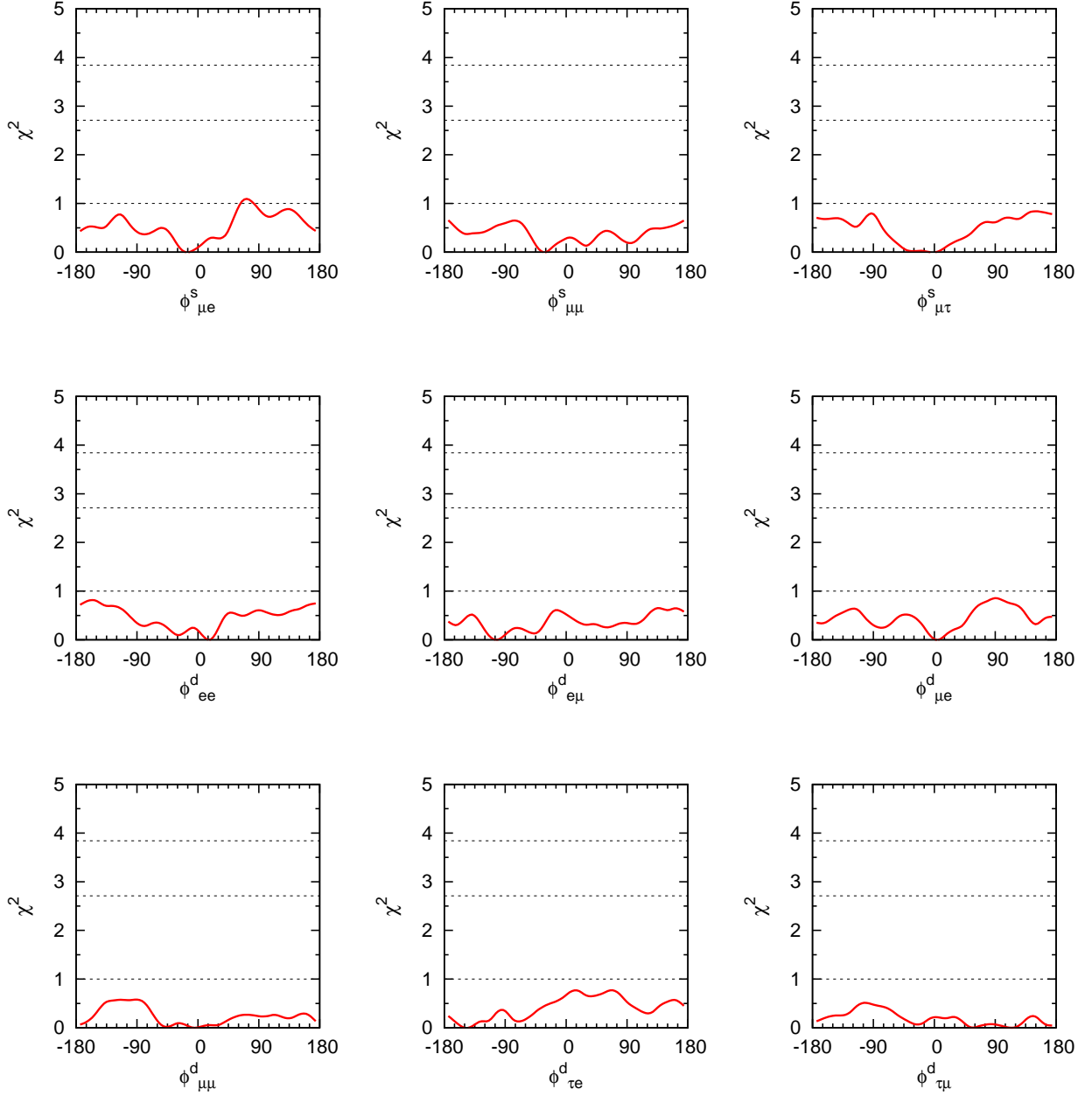


FIG. 9. Precision on the phases of the NSI parameters from ESSνSB data: χ^2 as a function of the test value of the NSI phases. The true values of the amplitudes of the NSI parameters are assumed to be half of their 90% C.L. bounds from Ref. [21], while the true values of the phases are taken to be zero. In each panel, all neutrino parameters (apart from the one indicated) have been marginalized over. The dotted lines from bottom to top show the 68%, 90% and 95% C.L., respectively.

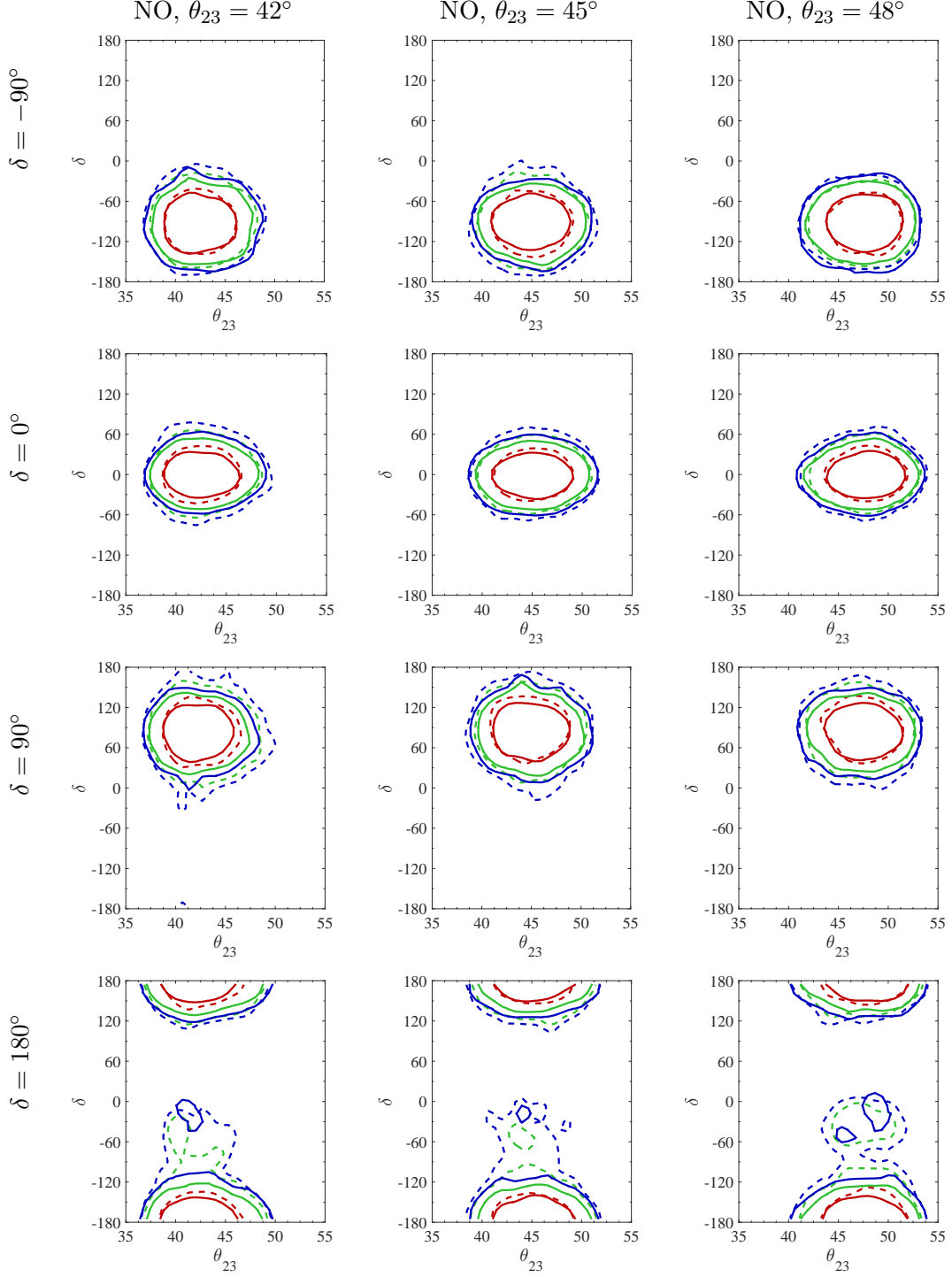


FIG. 10. Role of the near detector in precision measurements at ESS ν SB. Each panel shows the allowed region in the test $\theta_{23} - \delta$ plane, when the NSI parameters are taken to be non-zero in the data. The true values of the amplitudes of the NSI parameters are assumed to be half of their 90% C.L. bounds from Ref. [21]. The red, green and blue curves represent the 68%, 90% and 95% C.L. contours, respectively. The solid (dashed) contours show the allowed region with (without) the near detector.